Solution Blow Spun Poly(vinylpyrrolidone) Nanofibers Loaded with Atovaquone and Silver Nanoparticles for Wound Dressing Applications

Fahrettin Taha Ayvalı, Ali Kılıç

***Abstract*—**Chronic and diabetic wounds require dressings that control infection and support cell migration. Five poly(vinylpyrrolidone) nanofiber formulations (10% w/v in ethanol) were produced by solution blow spinning, with a silver nanoparticle (AgNP) stock at 15% v/v and atovaquone (ATQ) and hyaluronic acid (HA) stocks at 0 to 10% and 0 to 5% v/v. Mean fiber diameters ranged from 347 to 568 nm. Infrared spectra showed characteristic polymer bands. In human keratinocytes, only the formulation with the higher ATQ stock (S1) reduced viability significantly (≈88%), and all formulations remained above 70%. In a single scratch assay, wound closure after 18 h was 71.55% for S2 (lower ATQ stock) versus 41.66% for the control, whereas HA-containing formulations reduced closure. These results suggest that ATQ and HA content may modulate keratinocyte behavior.

***Index Terms*—**Atovaquone, Nanofiber Wound Dressing, Silver Nanoparticles, solution Blow Spinning

I. Introduction

Chronic wounds, including diabetic foot ulcers, heal slowly because persistent inflammation, impaired cell migration, and recurrent infection reinforce one another [1], [2]. Dressings for such wounds must therefore protect against infection and, at the same time, create a microenvironment that supports re-epithelialization. Recent dressing designs for diabetic wounds follow this principle by actively modulating the wound microenvironment [3].

Nanofibrous mats are attractive for this purpose because their fibrous architecture resembles that of the native extracellular matrix (ECM) and offers a high surface-area-to-volume ratio [4], [5]. Such mats can also carry antibacterial agents and drugs, and nanofibrous dressings that combine antibacterial activity with cytocompatibility and in vitro healing assays have been reported [6], [7]. Electrospinning is the most common fabrication route, but it requires a high-voltage electric field, and its throughput and suitability for handheld use are limited [8]. Solution blow spinning (SBS) instead draws the polymer solution into fibers with a pressurized gas stream [8], [9]. Because no high voltage is required, SBS can offer higher production rates than electrospinning [8], [9], and the fibers may be deposited directly onto a target such as a wound bed [8], [10]. SBS has been applied successfully to poly(vinylpyrrolidone) (PVP) [11]. The present work belongs to a project that aims to develop a portable SBS device for the direct application of drug-carrying dressings; the formulations reported here are candidate materials for that device.

PVP is a water-soluble polymer that interacts readily with metal surfaces [12] and is regarded as biocompatible [13]. Silver nanoparticles (AgNPs) are widely embedded in nanofibers to provide broad-spectrum antibacterial activity [14], [15], although their dose-dependent toxicity toward keratinocytes remains a concern [16]. Hyaluronic acid (HA), a glycosaminoglycan of the skin ECM, is frequently used to support wound healing [17]. Atovaquone (ATQ) is a clinically used antiparasitic drug [18], [19] that has been processed by electrospraying to improve its oral bioavailability [20]. In the present work, ATQ is considered an exploratory, repurposed anti-inflammatory candidate: it has been reported to inhibit signal transducer and activator of transcription 3 (STAT3) [21] and to reduce neutrophil infiltration in experimental colitis [22]. No wound-healing data for ATQ are available yet.

In a previous study, a Box–Behnken design (BBD) was used to optimize the SBS of neat PVP, and a polymer concentration of 10%, a feed rate of 10 mL/h, and an air pressure of 1.5 bar were predicted to give the smallest fibers (436.5 nm predicted, 442 nm measured) [23]. It remains to be established whether these conditions are suitable for PVP solutions that also contain ATQ, AgNPs, and HA, and how these components influence the response of skin cells. This study aimed to produce five AgNP-containing PVP formulations that differ in ATQ and HA content by SBS and to characterize their fiber morphology, infrared spectra, keratinocyte viability, and in vitro wound closure.

II. Materials and Methods

A. Materials

PVP (Kollidon 90, K-value ≈ 90; BASF, Ludwigshafen, Germany), ATQ, and HA were used as received. The AgNPs had a nominal particle size of 5 nm and were stabilized with trisodium citrate dihydrate. The solvent of the spinning

Manuscript received October 19, 2026. This work was supported by the TÜSEB Strategic R&D Project No. 35867 (program code 2023-B-02).

F. T. Ayvalı is with the Polymer Science and Technology Program, Istanbul Technical University, Istanbul, Türkiye

A. Kılıç is with the Department of Textile Engineering, Istanbul Technical University, Istanbul, Türkiye.

solutions was ethanol. The ATQ stock was prepared by dissolving 11 mg of ATQ powder in 128 mL of ethanol (≈85.9 µg/mL). The AgNP stock was aqueous (75 µg/mL), and the HA stock was an aqueous solution of 1% w/w (≈10 mg/mL). The human keratinocyte cell line HaCaT was cultured in high-glucose Dulbecco's modified Eagle's medium (DMEM). Dimethyl sulfoxide (DMSO), phosphate-buffered saline (PBS), and 3-(4,5-dimethylthiazol-2-yl)-2,5-diphenyltetrazolium bromide (MTT) were used as supplied.

B. Fabrication of the Nanofibers

Nanofibers were produced with a laboratory-scale SBS setup. PVP was dissolved at 10% w/v in ethanol, and the ATQ, AgNP, and HA stock solutions were added to the PVP solution as percentages of the final solution volume (% v/v). All components were mixed into a single solution and spun together. The polymer concentration (10% w/v), the solution feed rate (10 mL/h), and the air pressure (1.5 bar) were fixed at the values obtained from the previous BBD optimization of neat PVP [23]. Five formulations (S1–S5) were prepared at the stock percentages listed in Table I. The nominal content of each component in the fibers was calculated relative to the PVP mass, assuming complete retention; for example, 10% v/v of the ATQ stock gives 8.59 µg/mL ATQ in a solution containing 100 mg/mL PVP, i.e., 86 ppm. The ATQ stock content was limited to 10% v/v because higher contents led to polymer exit problems at the nozzle and heavy droplet formation in preliminary trials. The collected mats were stored at 4 °C in sealed bags until use.

TABLE I
COMPOSITION OF THE FORMULATIONS

Code	ATQ stock (% v/v)	AgNP stock (% v/v)	HA stock (% v/v)	ATQ in fiber (ppm)	Ag in fiber (ppm)	HA in fiber (wt%)
S1	10	15	0	86	112	0
S2	5	15	0	43	112	0
S3	5	15	1	43	112	0.10
S4	5	15	5	43	112	0.50
S5	0	15	0	0	112	0

Note: PVP was 10% w/v in ethanol in all samples. Stocks: ATQ, ≈85.9 µg/mL in ethanol; AgNP, 75 µg/mL in water; HA, 1% w/w (≈10 mg/mL) in water. Contents in the fibers are nominal, relative to the PVP mass, assuming complete retention of all components.

C. Scanning Electron Microscopy

The morphology of the mats was examined by scanning electron microscopy (SEM; VEGA 3, TESCAN, Brno, Czech Republic). Fiber diameters were obtained from 100 randomly selected fibers per sample and are given as mean ± standard deviation (SD).

D. Fourier-Transform Infrared Spectroscopy

Fourier-transform infrared (FTIR) spectra of a neat PVP mat (reference), pure ATQ, a PVP/ATQ mat (ATQ stock, 5% v/v), and an AgNP-containing PVP/ATQ mat were recorded between 4000 and 400 cm^{-1}. Bands of PVP were assigned according to [12] and bands of ATQ according to [20].

E. Cytotoxicity

HaCaT cells were seeded at 10^4 cells/well in 96-well plates and incubated for 24 h. The dressing materials (S1–S5) were sterilized with ultraviolet (UV) light and dissolved at 2 mg/mL in high-glucose DMEM. The old medium was removed, and 100 µL of the material-containing medium was added to the cells. Untreated cells served as the control. After 24 h of exposure, 10 µL of MTT solution (5 mg/mL) was added to each well, and the plates were incubated for 3–4 h at 37 °C and 5% CO_2 [24]. Formazan formation was checked by inverted light microscopy. The crystals were dissolved in 100 µL DMSO, and the absorbance was measured at 590 nm. Viability was expressed as a percentage of the untreated control. Cytotoxicity was judged against the criterion of the International Organization for Standardization (ISO) standard 10993-5, according to which a viability above 70% of the control indicates no cytotoxic effect [25], and against the 50% viability threshold used in the project.

F. Scratch Assay

HaCaT cells were seeded in 6-well plates at 5×10^5 cells/well and cultured for 24 h until they reached approximately 100% confluence. The cells were then treated with 2 mg/mL of the respective material, and a scratch was made in the monolayer with a sterile 200 µL pipette tip. Untreated cells served as the control, and no proliferation inhibitor was used. Detached cells were removed by washing with PBS. Images were acquired at 0 h and 18 h, and the cell-free areas were measured. Wound closure was calculated according to [3] as

$$\text{Closure (\%)} = \frac{A_0 - A_{18}}{A_0} \times 100 \quad (1)$$

where A_0 and A_{18} are the cell-free areas at 0 h and 18 h, respectively. The assay was performed once (n = 1).

G. Statistical Analysis

MTT viability values were compared by one-way analysis of variance (ANOVA) followed by Tukey's test. A p value below 0.05 was considered significant. Analyses were performed with GraphPad Prism 9. The MTT data are presented as mean ± SD of three replicates (n = 3). Fiber diameters are reported descriptively as mean ± SD, and the scratch-assay values (n = 1) are reported without statistical analysis.

III. RESULTS AND DISCUSSION

A. Fiber Morphology

SBS produced continuous, randomly oriented fiber mats from all five formulations (Fig. 1). The mean fiber diameters were 497 ± 125 nm (S1), 441 ± 174 nm (S2), 496 ± 182 nm (S3), 568 ± 168 nm (S4), and 347 ± 134 nm (S5) (Table II), all in the submicrometer range.

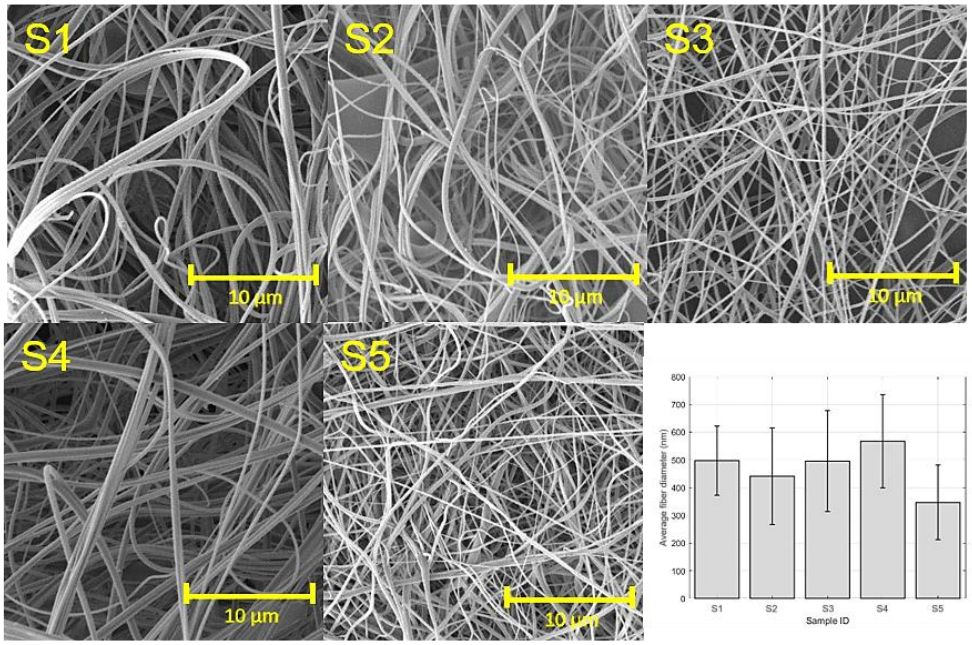


Fig. 1. SEM micrographs of the nanofiber mats S1–S5 (scale bars: 10 µm) and mean fiber diameters (bars: mean; error bars: SD). Compositions as in Table I.

TABLE II
MEAN FIBER DIAMETERS OF THE NANOFIBER MATS

Code	Fiber diameter (nm)
S1	497 ± 125
S2	441 ± 174
S3	496 ± 182
S4	568 ± 168
S5	347 ± 134

Because the diameter distributions overlap, the following trends are tentative. The mean diameter of S2 (441 nm) was close to that of neat PVP produced with the same settings in the previous optimization (442 nm) [23], whereas S5, which contained AgNPs but no ATQ, had the smallest mean diameter (347 nm). Doubling the ATQ stock content (S2 to S1) coincided with a larger mean (441 to 497 nm). Increasing the HA stock content (S2, S3, and S4: 0, 1, and 5% v/v) also coincided with larger means (441, 496, and 568 nm). A higher solution viscosity generally increases the fiber diameter in SBS [11], and dissolved HA may therefore contribute through a higher viscosity [26], [27]. In addition, the aqueous AgNP and HA stocks add 15–20% water to the ethanol solution (up to ≈20% in S4), which may contribute to the fiber-diameter differences, for example through changes in solvent evaporation and solution properties. In preliminary trials, the combination of several additives reduced the spinnability, which agrees with the view that spinnability in SBS is governed by solution viscosity and surface tension [9].

B. Fourier-Transform Infrared Analysis

The spectrum of the neat PVP mat (Fig. 2a) showed a broad O–H stretching band at ≈3394 cm^{-1}, which is attributed to absorbed water because PVP is hygroscopic [12]. Further bands were found at ≈2951 cm^{-1} (C–H stretching of the CH_2 groups), ≈1646 cm^{-1} (C=O stretching of the pyrrolidone ring, amide I), ≈1427 cm^{-1} (CH_2 bending, scissoring), ≈1279 cm^{-1} (C–N stretching), and ≈572 cm^{-1} (N–C=O bending) [12]. Pure ATQ is characterized by bands at 3369 cm^{-1} (O–H stretching), 2923 cm^{-1} (C–H stretching), 1642 cm^{-1} (C=O stretching), and 722 cm^{-1} (C–Cl) [20], and corresponding bands were found in the measured ATQ spectrum (Fig. 2b; the O–H band was labeled at ≈3378 cm^{-1}). In the PVP/ATQ mat (Fig. 2b), the PVP bands remained dominant (≈3394, ≈2951, and ≈1279 cm^{-1}), and the carbonyl band was labeled at ≈1642 cm^{-1}, i.e., ≈4 cm^{-1} below that of neat PVP. The ATQ-specific bands were not resolved in the fibers: the nominal ATQ content (43–86 ppm) is far below the sensitivity of FTIR, and the C=O band of ATQ (1642 cm^{-1}) lies within a few wavenumbers of the amide I band of PVP (1646 cm^{-1}).

The key question of the FTIR analysis was whether the addition of AgNPs alters the characteristic bands of PVP. The spectrum of the AgNP-containing PVP/ATQ mat (Fig. 2c) showed bands at ≈3412 (O–H), ≈1656 (C=O), ≈1423 (CH_2 bending), ≈1289 (C–N), and ≈572 cm^{-1} (N–C=O bending). Relative to neat PVP, the bands shifted by ≈+18 (O–H), ≈+10 (C=O), ≈−4 (CH_2), and ≈+10 cm^{-1} (C–N). Such small shifts may reflect an altered environment of the pyrrolidone carbonyl, for example through interaction with the Ag surface, which is a known coordination mode of PVP in the presence of metal nanoparticles [12], or through changes in the hydrogen bonding of absorbed water. The PVP bands were retained in the ATQ- and AgNP-containing fibers, and no new bands appeared, which gives no evidence of new covalent bonding. Because the nominal ATQ content is far below the sensitivity of FTIR, the spectra can neither confirm nor exclude the presence of ATQ in the fibers.

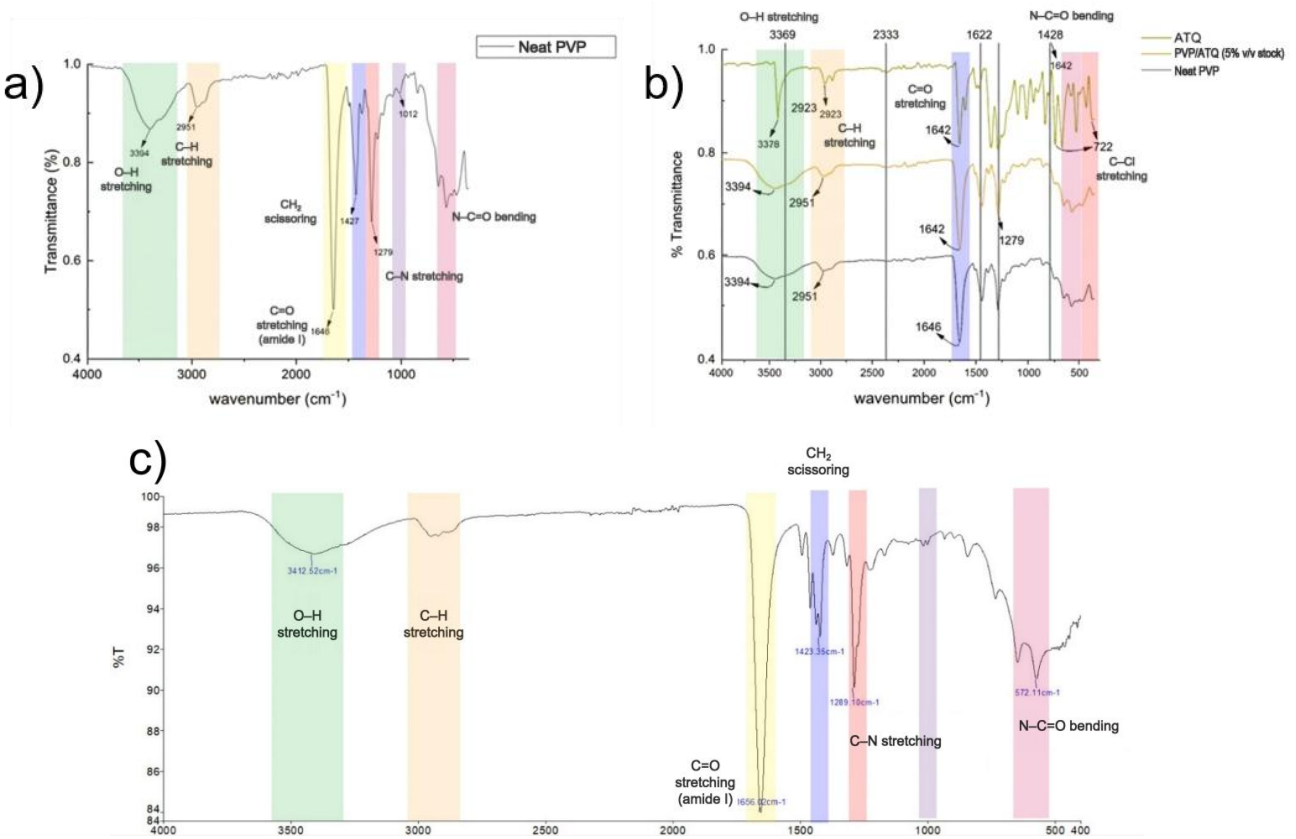


Fig. 2. FTIR spectra: (a) neat PVP nanofiber mat (reference) with band positions; (b) overlay of pure ATQ, the PVP/ATQ mat (ATQ stock, 5% v/v), and neat PVP; (c) AgNP-containing PVP/ATQ mat.

C. Cytocompatibility

Fig. 3 shows the viability of HaCaT cells after 24 h of exposure to 2 mg/mL of the dressing materials (n = 3). Only S1 (ATQ stock, 10% v/v) differed significantly from the control, with a viability of ≈88%, i.e., ≈8% below the control ($p < 0.05$). The viabilities of S2–S5 (≈89–91%, read from Fig. 3) did not differ significantly from the control ($p > 0.05$). This included the drug-free formulation S5 and both HA-containing formulations (S3 and S4). All formulations remained well above the 70% limit of ISO 10993-5 [25] and above the 50% threshold used in the project. Under the conditions tested, the materials may therefore be regarded as non-cytotoxic toward HaCaT cells. At 2 mg/mL, the nominal doses delivered to the cells were ≈0.22 µg/mL Ag for all samples and ≈0.17 µg/mL ATQ (≈0.47 µM) for S1 and ≈0.09 µg/mL ATQ (≈0.23 µM) for S2–S4, assuming complete retention (Table I). The small but significant decrease for S1, which was absent for S2–S4, may therefore indicate a dose-dependent effect of ATQ.

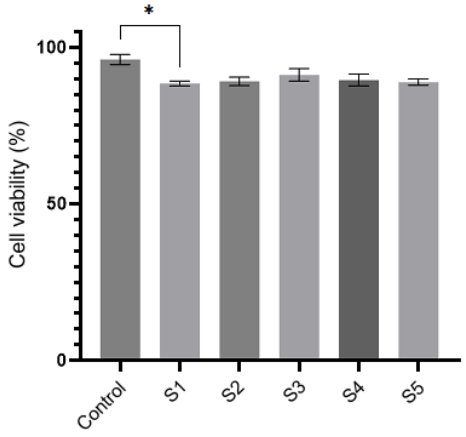


Fig. 3. Viability of HaCaT cells after 24 h of exposure to 2 mg/mL of the dressing materials (MTT assay); groups from left to right: control, S1, S2, S3, S4, and S5. Error bars: SD (n = 3). The asterisk marks a significant difference from the control (one-way ANOVA with Tukey’s test, $p < 0.05$).

D. In Vitro Wound Closure

The wound closure after 18 h is shown in Fig. 4 and Table III. Closure was 41.66% in the control group, 56.38% for S1, 71.55% for S2, 38% for S3, 6% for S4, and 11.88% for S5. S1 and S2 exceeded the control, S3 was close to it, and S4 and S5 were clearly below it. The micrographs (Fig. 4b) are consistent

with this ranking.

TABLE III
WOUND CLOSURE OF HACAT MONOLAYERS AFTER 18 H

Group	Wound closure (%)
Control	41.66
S1	56.38
S2	71.55
S3	38
S4	6
S5	11.88

Note: Each group was assayed once (n = 1). The values for S3 and S4 were read from the plotted data.

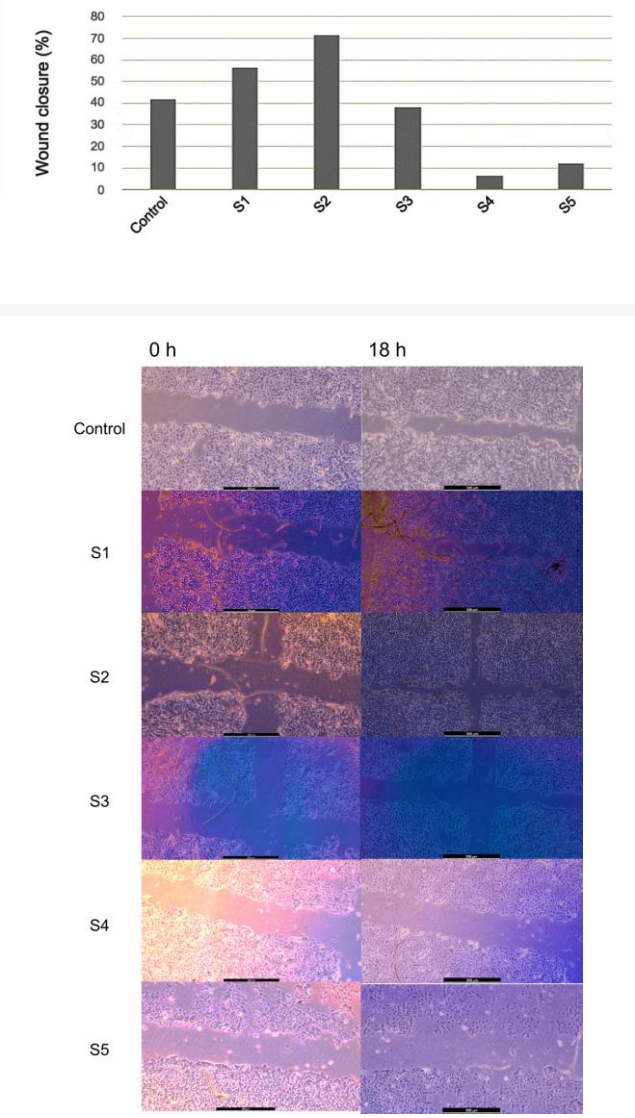


Fig. 4. Scratch assay with HaCaT cells (n = 1): (a) wound closure after 18 h for the control and the groups S1–S5; (b) phase-contrast micrographs at 0 h (left) and 18 h (right) for the control and S1–S5 (top to bottom; scale bar: 595 µm).

S2 and S5 differ only in the ATQ stock. The formulation containing only PVP and AgNPs closed 11.88% of the wound, whereas the same matrix with the 5% v/v ATQ stock closed 71.55%. This suggests that ATQ may counteract an inhibitory effect of AgNPs on closure, although the mechanism is unknown. Preliminary observations of the project indicated that a high AgNP level lowers migration. The response to ATQ was not monotonic, because S1 gave a lower closure than S2. This parallels the slight viability decrease of S1 in the MTT assay and suggests that the effective ATQ range may be narrow.

The closure decreased with increasing HA stock content (S2, S3, and S4), although the MTT assay showed no significant viability loss for S3 and S4. Overt cytotoxicity is therefore unlikely to be the only explanation. During the project, it was suggested that dissolved HA changes the composition of the culture medium and thereby impairs cell growth and migration. The effect of HA on keratinocyte migration may also depend on its molecular weight and concentration [28].

E. Limitations

The scratch assay was performed once (n = 1) and is descriptive; proliferation was not suppressed and may have contributed to closure [29]. ATQ is a mitochondrial complex III inhibitor [30] and the MTT assay reads mitochondrial reductase activity [31], so the small decrease for S1 may reflect metabolic inhibition rather than cell death. Cytotoxicity was assessed at one time point and one concentration, with the materials dissolved in the culture medium rather than extracted. The antibacterial activity of the dressings was not evaluated in this study. The dispersion of AgNPs and the content, integrity, and release of ATQ and Ag in the fibers were not characterized. Future work will include antibacterial testing of the dressings, release studies, time-resolved migration assays, and evaluation in a diabetic wound model.

IV. CONCLUSION

Five PVP nanofiber formulations containing AgNP, ATQ, and HA stock solutions were fabricated by SBS under conditions taken from a previous optimization and had mean fiber diameters of 347–568 nm. The FTIR spectra showed the characteristic PVP bands without new bands, whereas ATQ-specific bands were not resolved at the nominal ATQ content of 43–86 ppm. In HaCaT cells, all formulations maintained a viability above 70%, with only S1 showing a small but significant reduction. In the scratch assay (n = 1), S2 gave the highest wound closure at 18 h (71.55% versus 41.66% for the control), whereas the HA-containing formulations reduced closure. These results suggest that the ATQ and HA contents may modulate keratinocyte behavior and that S2 is a candidate for further antibacterial and in vivo evaluation.

REFERENCES

[1] V. Falanga *et al.*, “Chronic wounds,” *Nat. Rev. Dis. Primers*, vol. 8, no. 1, Art. no. 50, Jul. 2022, doi: 10.1038/s41572-022-00377-3. https://doi.org/10.1038/s41572-022-00377-3

[2] D. G. Armstrong, T.-W. Tan, A. J. M. Boulton, and S. A. Bus, “Diabetic foot ulcers: A review,” *JAMA*, vol. 330, no. 1, pp. 62–75, Jul. 2023, doi: 10.1001/jama.2023.10578. https://doi.org/10.1001/jama.2023.10578

[3] L. Cheng *et al.*, “A microenvironment-modulating dressing with proliferative degradants for the healing of diabetic wounds,” *Nat. Commun.*, vol. 15, no. 1, Art. no. 9786, Nov. 2024, doi: 10.1038/s41467-024-54075-7. https://doi.org/10.1038/s41467-024-54075-7

[4] Z. Zheng *et al.*, “Recent advances in structural and functional design of electrospun nanofibers for wound healing,” *J. Mater. Chem. B*, vol. 13, no. 18, pp. 5226–5263, 2025, doi: 10.1039/d4tb02718c. https://doi.org/10.1039/D4TB02718C

[5] X. Lu, L. Zhou, and W. Song, “Recent progress of electrospun nanofiber dressing in the promotion of wound healing,” *Polymers*, vol. 16, no. 18, Art. no. 2596, Sep. 2024, doi: 10.3390/polym16182596. https://doi.org/10.3390/polym16182596

[6] H. Adeli, M. T. Khorasani, and M. Parvazinia, “Wound dressing based on electrospun PVA/chitosan/starch nanofibrous mats: Fabrication, antibacterial and cytocompatibility evaluation and in vitro healing assay,” *Int. J. Biol. Macromol.*, vol. 122, pp. 238–254, Feb. 2019, doi: 10.1016/j.ijbiomac.2018.10.115. https://doi.org/10.1016/j.ijbiomac.2018.10.115

[7] M. Jahani *et al.*, “Antibacterial and wound healing stimulant nanofibrous dressing consisting of soluplus and soy protein isolate loaded with mupirocin,” *Sci. Rep.*, vol. 14, no. 1, Art. no. 26397, Nov. 2024, doi: 10.1038/s41598-024-78161-4. https://doi.org/10.1038/s41598-024-78161-4

[8] J. L. Daristotle, A. M. Behrens, A. D. Sandler, and P. Kofinas, “A review of the fundamental principles and applications of solution blow spinning,” *ACS Appl. Mater. Interfaces*, vol. 8, no. 51, pp. 34951–34963, Dec. 2016, doi: 10.1021/acsami.6b12994. https://doi.org/10.1021/acsami.6b12994

[9] E. S. Medeiros, G. M. Glenn, A. P. Klamczynski, W. J. Orts, and L. H. C. Mattoso, “Solution blow spinning: A new method to produce micro- and nanofibers from polymer solutions,” *J. Appl. Polym. Sci.*, vol. 113, no. 4, pp. 2322–2330, Aug. 2009, doi: 10.1002/app.30275. https://doi.org/10.1002/app.30275

[10] Z. Wen *et al.*, “In situ precision cell electrospinning as an efficient stem cell delivery approach for cutaneous wound healing,” *Adv. Healthc. Mater.*, vol. 12, no. 26, Art. no. 2300970, Oct. 2023, doi: 10.1002/adhm.202300970. https://doi.org/10.1002/adhm.202300970

[11] C. R. Cena, M. J. Silva, L. F. Malmonge, and J. A. Malmonge, “Poly(vinyl pyrrolidone) sub-microfibers produced by solution blow spinning,” *J. Polym. Res.*, vol. 25, no. 11, Art. no. 238, Nov. 2018, doi: 10.1007/s10965-018-1633-0. https://doi.org/10.1007/s10965-018-1633-0

[12] K. M. Koczkur, S. Mourdikoudis, L. Polavarapu, and S. E. Skrabalak, “Polyvinylpyrrolidone (PVP) in nanoparticle synthesis,” *Dalton Trans.*, vol. 44, no. 41, pp. 17883–17905, 2015, doi: 10.1039/C5DT02964C. https://doi.org/10.1039/C5DT02964C

[13] P. Franco and I. De Marco, “The use of poly(N-vinyl pyrrolidone) in the delivery of drugs: A review,” *Polymers*, vol. 12, no. 5, Art. no. 1114, May 2020, doi: 10.3390/polym12051114.

[14] A. L. Alfalluji, Q. S. Kadhim, and A. A. Mahdi, “Electrospun poly(ε-caprolactone)/silver nanoparticle nanofibrous scaffolds with antibacterial activity for wound-dressing applications,” *RSC Adv.*, vol. 15, no. 45, pp. 37899–37907, 2025, doi: 10.1039/d5ra06746d. https://doi.org/10.1039/D5RA06746D

[15] M. He *et al.*, “Electrospun silver nanoparticles-embedded feather keratin/poly(vinyl alcohol)/poly(ethylene oxide) antibacterial composite nanofibers,” *Polymers*, vol. 12, no. 2, Art. no. 305, Feb. 2020, doi: 10.3390/polym12020305. https://doi.org/10.3390/polym12020305

[16] L. Chen *et al.*, “Skin toxicity assessment of silver nanoparticles in a 3D epidermal model compared to 2D keratinocytes,” *Int. J. Nanomedicine*, vol. 14, pp. 9707–9719, Dec. 2019, doi: 10.2147/IJN.S225451. https://doi.org/10.2147/IJN.S225451

[17] M. F. Graça, S. P. Miguel, C. S. Cabral, and I. J. Correia, “Hyaluronic acid-based wound dressings: A review,” *Carbohydr. Polym.*, vol. 241, Art. no. 116364, Aug. 2020, doi: 10.1016/j.carbpol.2020.116364. https://doi.org/10.1016/j.carbpol.2020.116364

[18] J. P. Daily, A. Minuti, and N. Khan, “Diagnosis, treatment, and prevention of malaria in the US: A review,” *JAMA*, vol. 328, no. 5, pp. 460–471, Aug. 2022, doi: 10.1001/jama.2022.12366. https://doi.org/10.1001/jama.2022.12366

[19] A. Blanshard and P. Hine, “Atovaquone-proguanil for treating uncomplicated *Plasmodium falciparum* malaria,” *Cochrane Database Syst. Rev.*, vol. 2021, no. 2, Art. no. CD004529, Jan. 2021, doi: 10.1002/14651858.CD004529.pub3. https://doi.org/10.1002/14651858.CD004529.pub3

[20] A. Darade, S. Pathak, S. Sharma, and V. Patravale, “Atovaquone oral bioavailability enhancement using electrospraying technology,” *Eur. J. Pharm. Sci.*, vol. 111, pp. 195–204, Jan. 2018, doi: 10.1016/j.ejps.2017.09.051. https://doi.org/10.1016/j.ejps.2017.09.051

[21] M. Xiang *et al.*, “Gene expression-based discovery of atovaquone as a STAT3 inhibitor and anticancer agent,” *Blood*, vol. 128, no. 14, pp. 1845–1853, Oct. 2016, doi: 10.1182/blood-2015-07-660506. https://doi.org/10.1182/blood-2015-07-660506

[22] L. D. Manzanares *et al.*, “Atovaquone attenuates experimental colitis by reducing neutrophil infiltration of colonic mucosa,” *Front. Pharmacol.*, vol. 13, Art. no. 1011115, Oct. 2022, doi: 10.3389/fphar.2022.1011115. https://doi.org/10.3389/fphar.2022.1011115

[23] S. Küpoğlu and A. Toptaş, “Optimization of PVP nanofiber production via solution blow spinning using Box–Behnken experimental design,” presented at the 17th Int. Fiber and Polymer Research Symp., Yalova, Türkiye, May 15–16, 2026.

[24] T. Mosmann, “Rapid colorimetric assay for cellular growth and survival: Application to proliferation and cytotoxicity assays,” *J. Immunol. Methods*, vol. 65, no. 1–2, pp. 55–63, Dec. 1983, doi: 10.1016/0022-1759(83)90303-4. https://doi.org/10.1016/0022-1759(83)90303-4

[25] *Biological Evaluation of Medical Devices — Part 5: Tests for In Vitro Cytotoxicity*, ISO 10993-5:2009, International Organization for Standardization, Geneva, Switzerland, 2009.

[26] M. Séon-Lutz, A.-C. Couffin, S. Vignoud, G. Schlatter, and A. Hébraud, “Electrospinning in water and in situ crosslinking of hyaluronic acid / cyclodextrin nanofibers: Towards wound dressing with controlled drug release,” *Carbohydr. Polym.*, vol. 207, pp. 276–287, Mar. 2019, doi: 10.1016/j.carbpol.2018.11.085.

[27] Z. Liu, S. Ramakrishna, I. Ahmed, C. Rudd, and X. Liu, “Rheological, surface tension and conductivity insights on the electrospinnability of poly(lactic-co-glycolic acid)-hyaluronic acid solutions and their correlations with the nanofiber morphological characteristics,” *Polymers*, vol. 14, no. 20, Art. no. 4411, Oct. 2022, doi: 10.3390/polym14204411. https://doi.org/10.3390/polym14204411

[28] Y. Kawano *et al.*, “Wound healing promotion by hyaluronic acid: Effect of molecular weight on gene expression and in vivo wound closure,” *Pharmaceuticals*, vol. 14, no. 4, Art. no. 301, Mar. 2021, doi: 10.3390/ph14040301. https://doi.org/10.3390/ph14040301

[29] A. Grada, M. Otero-Vinas, F. Prieto-Castrillo, Z. Obagi, and V. Falanga, “Research techniques made simple: Analysis of collective cell migration using the wound healing assay,” *J. Invest. Dermatol.*, vol. 137, no. 2, pp. e11–e16, Feb. 2017, doi: 10.1016/j.jid.2016.11.020. https://doi.org/10.1016/j.jid.2016.11.020

[30] F. Mudassar, H. Shen, G. O’Neill, and E. Hau, “Targeting tumor hypoxia and mitochondrial metabolism with anti-parasitic drugs to improve radiation response in high-grade gliomas,” *J. Exp. Clin. Cancer Res.*, vol. 39, no. 1, Art. no. 208, Oct. 2020, doi: 10.1186/s13046-020-01724-6. https://doi.org/10.1186/s13046-020-01724-6

[31] M. Ghasemi, T. Turnbull, S. Sebastian, and I. Kempson, “The MTT assay: Utility, limitations, pitfalls, and interpretation in bulk and single-cell analysis,” *Int. J. Mol. Sci.*, vol. 22, no. 23, Art. no. 12827, Nov. 2021, doi: 10.3390/ijms222312827. https://doi.org/10.3390/ijms222312827